1524 *Macromolecules* **2010**, *43*, 1524–1529
DOI: 10.1021/ma901755v

Macromolecules
ARTICLE

Phase Behavior of Thin Film Brush-Coated Nanoparticles/Homopolymer Mixtures

Jenny Kim and Peter F. Green*

Department of Materials Science and Engineering, University of Michigan, Ann Arbor, Michigan 48109

Received August 5, 2009; Revised Manuscript Received December 17, 2009

ABSTRACT: The phase behavior of supported thin film mixtures ($h \sim 120$ nm thick) of polystyrene (PS) brush-coated spherical nanoparticle and PS homopolymers is characterized by three regimes, depending on P, the degree of polymerization of the PS host, and N, the degree of polymerization of the grafted chains. Phase separation between the nanoparticles and the host chains occurs in samples for which $N < N^*$ and $P \gg N$. Specifically, the nanoparticles segregate exclusively at the substrate and free surface in these samples, forming a trilayered structure. When $P \gg N$ and $N > N^*$, preferential segregation of the grafted nanoparticles to the interfaces is accompanied by a structural instability (surface roughening). We identify this as regime I and the former as regime II. The system is miscible in regime III ($P < N$ and $N > N^*$); the nanoparticles are dispersed throughout the film. There exists a region of partial miscibility that separates regimes I and III. The characteristics of regime I are reminiscent of phase separation in polymer/polymer thin film mixtures. Regime II is reminiscent of the interfacial segregation of hard spheres in an athermal melt of polymer chains.

Introduction

Polymer nanocomposites (PNCs) are a technologically important class of materials, with structural, biomedical, and optoelectronic applications.[1−3] Depending on the polymer host and nanoparticle functionalities, this class of materials may exhibit properties, such as thermal, mechanical, and optical, that differ significantly from the pure polymer host, even at low nanoparticle concentrations.[3−5] The properties of PNCs are sensitive to their microstructural features, which are generally difficult to control, largely due to a complex interplay of entropic and enthalpic interactions that determine the spatial distribution of nanoparticles.[4,6] One successful strategy that has been used to control the phase behavior of these systems is to graft chains, chemically identical to the melt chains, onto the nanoparticle surfaces.[4,6] In principle, control of the degree of polymerization of the grafted chains, N, the degree of polymerization of the host, P, nanoparticle core radius, R_c, composition, and the grafting density, σ, would enable control of the phase behavior and hence the properties of the system.[4,6] The phase behavior of thin film mixtures polystyrene (PS) chain grafted gold nanoparticles with PS homopolymer chains is of particular interest in this paper.

The miscibility between brush-coated nanoparticles and a melt of chains, chemically identical to the grafted chains, is determined primarily by entropic constraints. The translational entropy promotes dispersion of the spherical particles in the system. For spherical particles of diameter D in a melt, the entropy of mixing is $F_{mix} \sim (\phi/D^3)\ \ln \phi$, where ϕ is the volume fraction; mixing is favored with decreasing D.[7,8] When chains are grafted onto the nanoparticles, the chains from the melt may be excluded from the brush layer at sufficiently high grafting densities. This would favor aggregation of the particles in order to reduce the interfacial free energy associated with the brush/host chain interfaces. There is an additional driving force; attraction between the nanoparticles might occur because the melt chains confined between particles suffer a loss of conformational entropy. This loss increases with increasing P, which would have the effect of enhancing particle−particle aggregation for larger P. At lower grafting densities, and $P/N > 1$, interpenetration of the brush layer by the free host chains may occur, and this would favor dispersion of the particles within the host.

The curvature of the particle surface has an important influence on the nanoparticle/host chain interpenetration and hence miscibility. Klos et al. calculated density profiles for small nanoparticles, $R_c < N^{1/2}a$, where a is the size of a monomer, as a function of distance from particle surfaces for a wide range of values of R_c, N, σ, and P.[9] It was shown that as R_c decreases, the grafted chains became less stretched, due to reduced crowding, for a constant σ and P.[10,11] The probability of interpenetration by the host chains into the brush layer therefore increases with decreasing particle radius. Hence, particle dispersion is therefore favored under these circumstances.

In thin films, miscibility is determined by additional factors that include melt/interface and nanoparticle/interface and melt/nanoparticle interactions. Recently, Meli et al. showed that it was possible to disperse the nanoparticles within the polymer host and, additionally, to induce the nanoparticles to reside exclusively at the interfaces, free surface, and substrate, through control of N and P.[12] Specifically, for small gold nanoparticles of $R_c = 1.8$ nm ($R_c \ll N^{1/2}a$) and $N = 10$ ($R = 2(R_c + R_N) \sim 4.5$ nm), the nanoparticles were miscible with PS host chains of $P = 125$, whereas for $R_c = 2.5$ nm and $N = 10$ ($D = 7.5$ nm), the nanoparticles phase separated toward the interfaces; the interior was virtually devoid of nanoparticles. However, when $N = 480$, the system was miscible largely due to interpenetration between the melt chains of $P = 125$ and the grafted chains. These observations were rationalized in terms of the foregoing melt/brush interaction scaling arguments.

In this paper we examine the phase behavior of thin film mixtures of $\phi \sim 2-5$ wt % gold nanoparticles ($R_c = 2.5$ nm), onto which PS chains of varying N were grafted, and *entangled* PS chains of varying P. A phase diagram, which shows qualitatively the location of miscible, partially miscible, and immiscible regions, depending on N and P (at constant σ) is proposed for

*To whom correspondence should be addressed.

 Published on Web 01/07/2010

this system. We show that the phase behavior of supported thin film ($h = 120 \pm 10$ nm) PS brush-coated spherical nanoparticle/PS homopolymer mixtures is characterized by three regimes, depending on P and N. For $P \gg N > N^*$, complete phase separation occurs, wherein the nanoparticles segregate to both interfaces, accompanied by a structural instability. The topography of the film is characterized by spatial fluctuations in height. We will identify this as regime I. When $P \gg N$ and $N < N^*$, phase separation occurs only normal to the substrate; the nanoparticles reside exclusively at the interfaces, and the sample is characterized by a trilayer structure. This is the regime discussed by Meli et al. and is identified in this paper as regime II. For $P/N < 3$ and $N > N^*$, the system is miscible, wherein the nanoparticles are dispersed throughout the sample; this is regime III. There is a transition between regimes I and III, where nanoparticles and host chains are partially miscible. The characteristics of phase separation in regime I are similar to those of thin film polymer/polymer blends, whereas those of regime II are similar to the phase separation of hard spheres in an athermal melt with homopolymer chains.

Experimental Section

The gold nanoparticles (AuNPs) were synthesized through modification of a two-phase precipitation method described elsewhere.[4,6] The thiol-terminated PS molecules (PS-SH) were purchased from Polymer Source ($M_n = 1000$ g mol^{-1}, $M_w/M_n = 1.4$; $M_n = 29\,000$ g mol^{-1}, $M_w/M_n = 1.08$; $M_n = 50\,000$ g mol^{-1}, $M_w/M_n = 1.06$). The synthesized particles were cleaned 10 times using methanol and toluene to remove excess ligands in the solution. After cleaning, the particles were dried, completely, and dissolved in toluene. Thermogravimetric analysis (TGA) was used to obtain the weight fractions of gold and ligands. The runs were performed by TA 2960 instrument under air at the heating rate 5 °C/min. Using the weight fractions, the average particle size, determined from scanning transmission microscopy (STEM), and the densities of each species, we were able to calculate, for the $M_n = 50\,000$ g mol^{-1} ligand, the areal grafting density, $\sigma = 1.44$/nm^2 and $R_{NP} = 27.0$ nm, with the R_c (radius of core) $= 2.42 \pm 0.61$ nm and R_N (brush thickness) $= 12.3$ nm.[12,13] R_{NP} was calculated from the interparticle spacing considering that chain-grafted particles are closely packed. Throughout the remainder of this paper the gold nanoparticles are identified as $AuPS_N$, where N is the degree of polymerization of the grafted chain. While results for $AuPS_{480}$ are mainly discussed, $AuPS_{10}$, $AuPS_{115}$, and $AuPS_{280}$ particles have been synthesized with the sizes 5.0, 4.65, and 4.81 nm and $\sigma = 1.44$, 1.54, and 1.48 chains/nm^2, respectively.

Sample Preparation. A series of toluene/PS solutions, each containing 3 wt % PS of different monodisperse molecular weights ($M = 170\,000$ g/mol ($P = 1630$); 400 000 g/mol ($P = 3840$); 590 000 g/mol ($P = 5660$); and 900 000 g/mol ($P = 8640$)), were mixed with $AuPS_{480}$ nanoparticles, of concentrations 2−5 wt %; the mixtures were stirred for at least 30 min. The solutions are then spin-cast onto cleaned SiO_x/Si substrates to form films with thicknesses of approximately 110−130 nm. The thicknesses of the samples were determined using spectroscopic ellipsometry (M-44, J.A. Woollam Co.).

Samples were annealed in a vacuum oven at 65 °C for a day for solvent evaporation and then annealed in compressed CO_2 ($T = 50$ °C, $P = 13.8$ MPa) in a high-pressure cell. The annealing procedure is described in detail elsewhere.[14] Supercritical CO_2 is a poor solvent for PS, and it plasticizes the mixture enabling the system to reach equilibrium. It is used here in order to avoid heating the sample to very high temperatures to achieve a reasonable degree of plasticization and maintain thermal stability of grafted chains. Additionally sc-CO_2 annealing is more controllable than liquid solvent annealing.

Transmission electron microscopy (TEM), using a JEOL-2010F in scanning mode (STEM), was used to characterize the lateral distribution of the nanoparticles in the samples. STEM was used to characterize the Au NP distribution throughout the film before and after annealing. The STEM samples were prepared first by spin-casting the solutions onto a glass slide and then floating the resulting film from the slide onto a bath of distilled water. The films were then deposited from the water bath onto silicon nitride windows (SPI Supplies) for STEM analysis. Images were taken using high annular angle dark field (HAADF) detector (Z-contrast) applying an accelerating voltage of 200 kV.

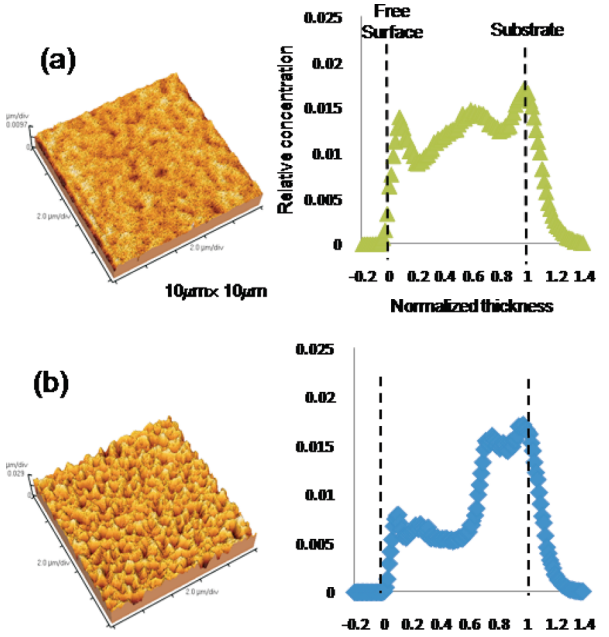

Figure 1. Topographies and corresponding depth profiles of Au for a 4 wt % $AuPS_{480}/PS_{8640}$ films are shown here for (a) as-cast films and (b) CO_2 annealed films at 50 °C, 13.8 MPa for 4320 min.

Depth profiles of AuNPs within the PS films were acquired using DSIMS, performed by Dr. Tom Mates at the University of California, Santa Barbara, using a Physical Electronic 6650 Quadropole instrument. The combination of STEM and SIMS enabled determination of the spatial distribution of nanoparticles in the films. Topographical analyses were determined using Autoprobe CP scanning force microscopy (SFM), operating in the contact mode. Information about rms roughness (R_q) and kurtosis were extracted by WSXM software in order to characterize the topography. The characteristic lengths were obtained from the power spectrum density (PSD), which characterizes the surface fluctuations, as a function of frequency.

Results and Discussion

The SFM measurements indicate that the $AuPS_{480}/PS_{8640}$ films, $h \approx 120$ nm, exhibited surface roughening, as shown in Figure 1a for $P = P_0 = 8640$ and $N = 480$. The roughening increased after annealing (Figures 1b). The depth profiles of the gold particles in Figure 1a,b exhibit maxima at the free surface and at the polymer/substrate interface. These maxima represent enhanced interfacial segregation of brush-coated Au nanoparticles. This segregation may be understood in analogy to multiarm star molecules at interfaces; chains tethered to the particles suffer less of an entropy penalty upon segregation to an interface than the linear host chains. This relieves frustrated packing in the bulk; it also relieves the entropic restrictions associated linear chains at flat interfaces. The surface roughening is similar to the behavior of phase-separated polymer/polymer thin film mixtures.[15,16]

Characteristics of the structure of the phase separated samples will be discussed below, but in the meantime we note that samples

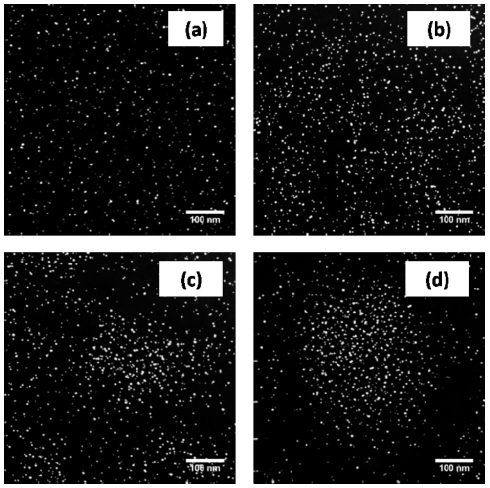

Figure 2. STEM images are shown for 4 wt % $AuPS_{480}$ mixed with PS hosts different molecular weights: (a) M_n(PS) = 170 kg/mol (P = 1630); (b) M_n(PS) = 400 kg/mol (P = 3840); (c) M_n(PS) = 590 kg/mol (P = 5660); (d) M_n(PS) = 900 kg/mol (P = 8640).

for which $P_0 > 8N$ exhibit this behavior: preferential nanoparticle segregation to the interfaces accompanied by a structural instability. We will associate this behavior with regime I. The structural instability is suppressed in the range of N and P where $3N < P_0 < 8N$. However, while the instability is suppressed, phase separation still occurs; the nanoparticles segregate exclusively to the interfaces. This behavior is associated with regime II and was identified by Meli et al.; it is analogous to phase separation between the homopolymers and athermal hard sphere nanoparticles. When $P < 3N$, the system is miscible; this behavior is associated with regime III. A "phase diagram" characterizing the behavior of this system, depending on N and P, will be discussed later.

The features of phase separation in regime I are now discussed. In-plane distributions of AuNPs in hosts of different P, and fixed N = 480, for as-cast films are shown in Figure 2. The particle-rich and particle-poor regions are evident from the images. The images indicate that as P increases from 1630 (3.4N) to 8640, the particles aggregate and the extent of aggregation increases with increasing P.

Information about phase separation of the system may be learned from an analysis of the number of nanoparticles throughout different regions of the sample. The average number of particles in the particle-rich phase, N_{par}, and in the polymer-rich phases, N_{poly}, were determined for each sample by counting the number of particles in several selected areas of each sample; the results are plotted in Figure 3. In this figure, $r = N_{par}/N_{poly}$; $r \sim 1.0$, increases from $P \sim 3840$, to $r \sim 3.3$, for $P \sim 8640$ (Figure 3). $P \sim 1630$ denotes the transition from miscibility to partial miscibility, with increasing P; the system is immiscible for $P >$ ~4000. This transition miscibility to immiscibility occurs within the range of $3N < P < 8N$.

Surface topographies of the $AuPS_{480}$/PS samples were also examined, using the power spectrum density analysis, to learn more about phase separation (Figure 4). The PSD exhibited a much larger maxima for the sample containing 4% $AuPS_{480}/PS_{8640}$ than the sample containing 2% $AuPS_{480}/PS_{8640}$, revealing a much larger degree of phase separation (Figure 4a). Further, the PSD maxima and the average wavelength of the fluctuations in the 4% $AuPS_{480}/PS_{5660}$ sample were appreciably smaller than that of the 4% $AuPS_{480}/PS_{8640}$ sample, reflecting a much smaller degree of phase separation. This observation is consistent with the data in Figure 2.

The rms roughnesses of samples containing 2% and 4% $AuPS_{480}$/PS are shown in Figure 4b. The rms roughness increased

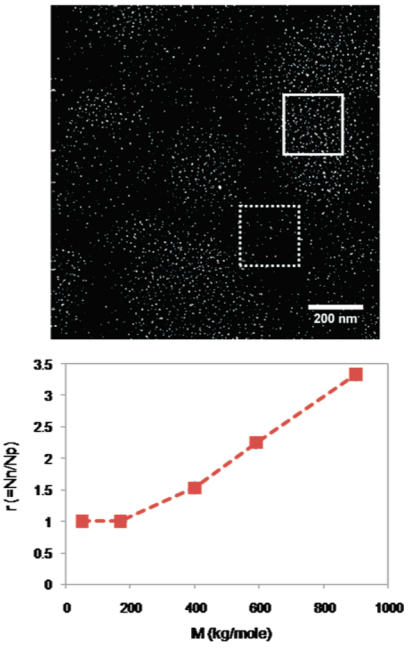

Figure 3. Ratio $r = N_{par}/N_{poly}$ is plotted as a function of the molecular weight of the PS host chains. 200 × 200 nm^2 areas were analyzed throughout different regions of the samples. The number of particles at the boundary is $(N_{par} + N_{poly})/2$.

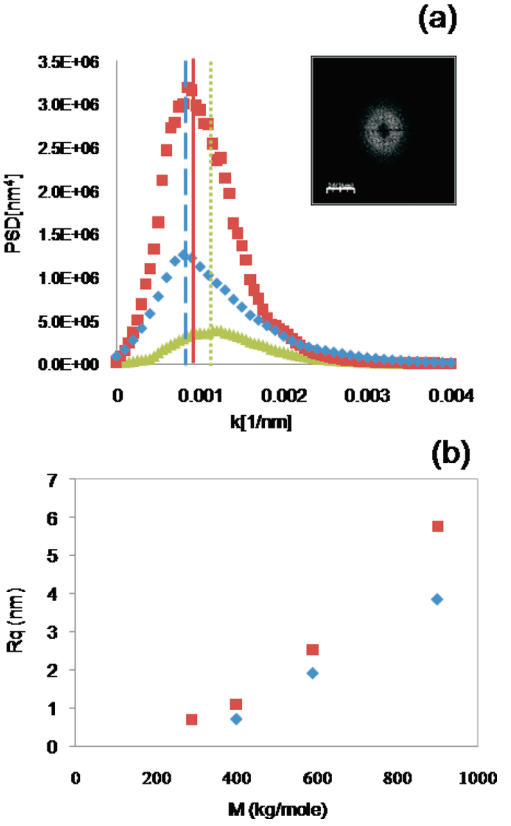

Figure 4. (a) Power spectrum densities of different samples (red square: 4% $AuPS_{480}/PS_{8640}$; blue diamond: 2% $AuPS_{480}/PS_{8640}$; green triangle: 4% $AuPS_{480}/PS_{5660}$) are shown here. The lines represent the characteristic wave vector for each mixture. (b) The rms roughness (R_q) vs M_n are plotted for various host chain lengths.

with increasing P, reflecting increasing phase separation. The sample with the higher concentration exhibited larger surface fluctuations, again reflecting increasing phase separation.

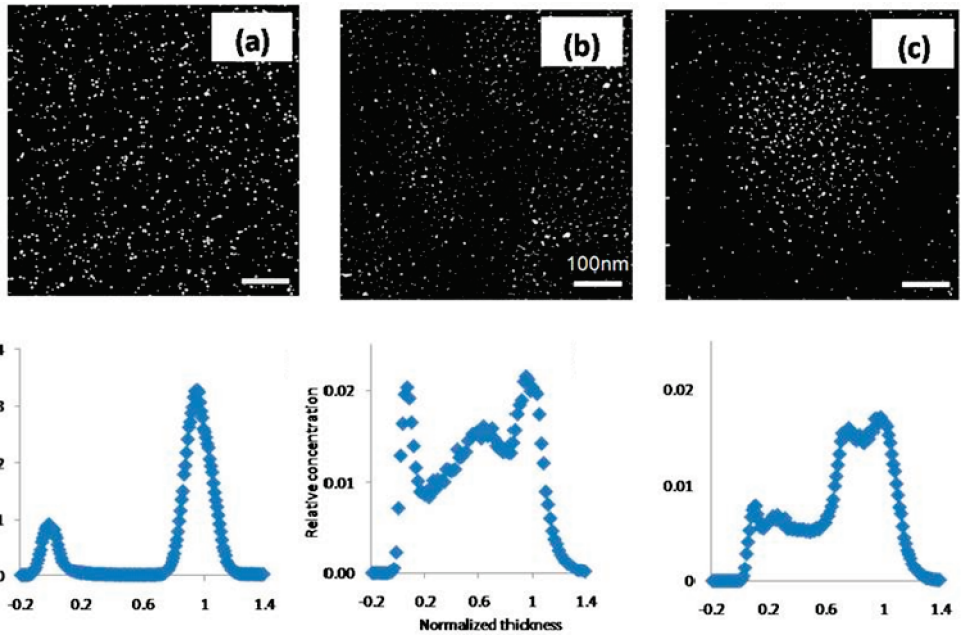

Figure 5. STEM images and depth profiles are shown here for samples in which $P = 8640$ and (a) $N = 10$, (b) $N = 280$, and (c) $N = 480$. All samples contained 4 wt % Au.

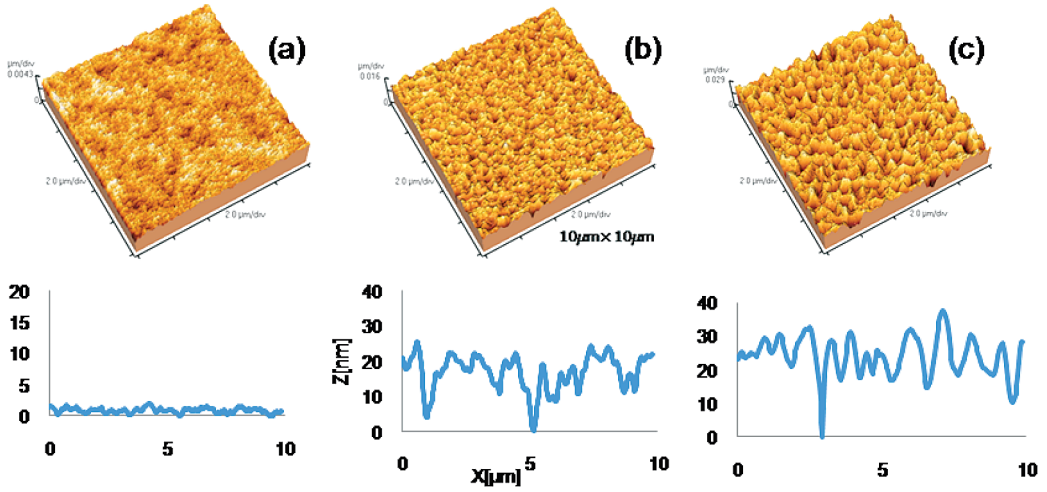

Figure 6. The corresponding topographies are shown here for the samples in Figure 5.

Note that for host $P < 4000$ the surfaces are effectively smooth. However, for greater values of P, the surface fluctuations increased rapidly. Again, this latter regime is associated with enhanced lateral phase separation.

Based on the AFM and STEM data, the regions of high nanoparticle concentration (aggregation) are associated with the peak locations of the surface topographies. The development of the topography reflects phase separation of the system, analogous to polymer/polymer phase separation in thin films; phase separation becomes significant at large P. The final state of these sample is one in which an excess of nanoparticles resides at both interfaces. The peaks and valleys in the topographies represent an attempt by the system to minimize the area of contact between the long chain grafted ($N = 480$) nanoparticles and the homopolymer chains, subject to the interfacial constraints. Finally, with regard to experimental details, we note that the state of dispersion of the particles did not change significantly from the in-plane view after annealing for longer times, up to 4320 min, as one might anticipate if the phase separation were nearly complete.

The distinction between phase separation phenomena in regimes I and II is clearly illustrated in Figures 5 and 6. It is clear from the STEM images in Figure 5a−c that as N increases, for these mixtures containing PS of $P = 8640$, the particle aggregation increases. The SIMS profiles show that for smaller N, the nanoparticles reside exclusively at the interfaces. With increasing N, there is evidence of nanoparticles in the interior of the sample. However, the AFM images in Figure 6 provide the best insight into the actual phenomenon. The surface of the sample of lowest N is relatively smooth, whereas with increasing N, the surfaces exhibit significant height fluctuations. The images in Figures 5 and 6 show that for small N the particles reside exclusively at the interfaces and the surfaces are smooth. However, at large N, a structural instability accompanies the interfacial segregation, reflecting the behavior of polymer/polymer thin film systems that undergo phase separation.

Parenthetically, for $P/N \gg 1$, one might anticipate that the nanoparticles would be miscible with the melt chains, particularly for sufficiently small values of N and R_c. Under such conditions

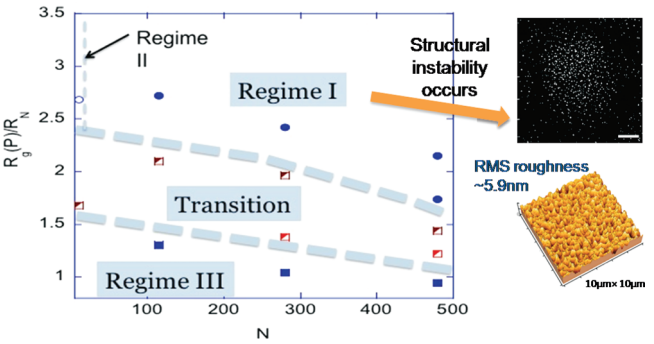

Figure 7. Phase diagram, represented by $R_g(P)/R_N$ vs N, is shown here for samples characterized for various values of N and P.

particles may be incorporated within the host without much loss of conformational entropy. Such a case was observed by Meli et al. when particle diameter was $D_{NP} = 4$ nm ($R_c = 0.9$ nm) and $P = 8640$. In our experiments, nanoparticles were larger, $D = 10$ nm, and this behavior was not observed.

The N-dependence of the phase behavior of AuPS$_N$/PS, described above, is associated with three competing entropic contributions to the free energy. While grafted chains pack densely around the particle core to minimize the entropic stretching energy, the grafted chains reside in more stretched state for smaller N, in order to accommodate the high grafting density ($\sigma > 1$) near the surface of the core. Therefore, with decreasing N, at constant σ, the host chains are excluded from the brush layer. Consequently, the particles exhibit a larger tendency to segregate to minimize the interfacial free energy. Segregation is further favored, as mentioned earlier, because confinement of the chains between nanoparticles reduces the conformational entropy of the host chains; this effect increases with increasing P. The competing effect is that the host chain/brush layer interfacial tension decreases with decreasing N (and decreasing R_{NP}), which favors miscibility and hence dispersion. Therefore, the suppression of the instability is not unexpected with decreasing N at constant P.

A "phase" diagram was developed to qualitatively delineate the different regimes based on N and P at constant σ (Figure 7). The broken lines in the diagram show qualitatively where the different regimes of phase separation, miscibility, and partial miscibility occur. For large values of N and P, the system is incompatible and phase separation occurs in a manner similar to phase separation in polymer/polymer systems (regime I). When N is sufficiently small ($N < N^* = 10$), the behavior is that of hard particles segregating to the interfaces to minimize the free energy of the system. There is a transition regime of partial miscibility between regime I and regime III, where the system is miscible. We anticipate that the quantitative aspects of the phase diagram are specific to the polymer and the molecular weights. However, we expect that the qualitative aspects of this phase diagram should be general, assuming that the nanoparticle is not too small.

We now make final comments regarding the phase separation in regimes I and II by drawing an analogy with the behavior of homopolymer/micelle systems. Semenov et al. proposed a theory of phase behavior of a linear homopolymer chain, A, and copolymer, A−B, spherical micelles (A−B/A) mixture.[17,18] The relative sizes of N_{A-B} to N_A determine, in part, the size of the micelle and the phase stability. When $N_{A-B} \gg N_A$, separation into A−B micelle-rich and homopolymer-rich phases occurs due to an attraction between micelles. For thin film A−B micelle/A homopolymer mixtures, micelles segregated toward the interfaces.[17,19] The attraction between the micelles was predicted to increase with the size of the micelles.[17,19,20] Though this comparison between micelle/homopolymer mixtures was qualitative, one may qualitatively anticipate the phase behavior and structure of AuPS/PS mixtures based on parameters N, P, and D ($2R_c + 2R_N$). The SIMS image in Figure 1 shows four maxima, each of which is associated with a layer of brush-coated nanoparticles. The diameter of the nanoparticles is approximately $D = 30$ nm, and the depth resolution of the SIMS measurement is just under 20 nm. The two peaks near the substrate correspond to the spacing of two layers of nanoparticles. It is difficult to make the same assessment of the free surface due to the instability. Nevertheless, the spacing between the peaks near the free surface and the substrate is also consistent with two layers of grafted nanoparticles. The central region corresponds to homopolymer chains. The theory of Semenov indicates that the attraction of micelles, and by extension our brush-coated particles, should be strong. This would be consistent with the interpretation of the maxima in the SIMS data. Finally, we note that with regard to athermal mixtures of stars and linear chains, where only differences in architecture are considered, Fredrickson et al. predicted that they are intrinsically, thermodynamically, less stable than linear−linear athermal mixtures.[21] This prediction is consistent with our findings in regime I.

Conclusions

Phase separation of thin film brush-coated NPs/homopolymer mixture was systematically studied by changing ϕ, N, and P at a fixed brush density and nanoparticle core radius. We showed that the phase behavior of supported thin film PS brush-coated spherical nanoparticle/PS homopolymer mixtures is characterized by three regimes, depending on P and N. Regime I is characterized by phase separation between the nanoparticles and the host chains normal to the substrate, accompanied by a structural surface instability. With decreasing P, at fixed N, the system became fully miscible for $P/N < 3$ (regime III). The system was partially miscible between regimes I and III. Regime II was observed when $N < N^*$ and sufficiently large P; phase separation occurred normal to the substrate, but the instability was suppressed. Characteristics of regime I are reminiscent of the behavior of thin film polymer/polymer mixtures. The behavior in regime II is characteristic of the behavior of hard spheres separating from an athermal mixture with polymer chains.

Acknowledgment. This research was supported by the U.S. Department of Energy, Office of Science, DOE#DE-FG02-07ER46412.

References and Notes

(1) Jia, J.; Wang, B.; Wu, A.; Cheng, G.; Li, Z.; Dong, S. *Anal. Chem.* **2002**, *74* (9), 2217–2223.
(2) Yu, G.; Gao, J.; Hummelen, J. C.; Wudl, F.; Heeger, A. J. *Science* **1995**, *270* (5243), 1789–1791.
(3) Bhattacharya, P.; Ghosh, S.; Stiff-Roberts, A. D. *Annu. Rev. Mater. Res.* **2004**, *34* (1), 1.
(4) Abraham, A.; Luciana, M.; Peter, F. G. *Nano Lett.* **2008**, *8* (8), 2271.
(5) Mackay, M. E.; Ho, D. L.; Ho-Cheol, K.; Hawker, C. J.; Dao, T. T.; Van Horn, B.; Tuteja, A. *Nat. Mater.* **2003**, *2* (11), 762.
(6) Oh, H.; Green, P. F. *Nat. Mater.* **2009**, *8* (2), 139–143.
(7) Lee, J. Y.; Shou, Z. Y.; Balazs, A. C. *Macromolecules* **2003**, *36* (20), 7730–7739.
(8) Lee, J.; Buxton, G.; Balazs, A. *J. Chem. Phys.* **2004**, *121* (11), 5531.
(9) Xu, J. *J. Polym. Sci., Part B: Polym. Phys.* **2006**, *44* (19), 2811–2820.
(10) Klos, J.; Pakula, T. *J. Chem. Phys.* **2003**, *118* (16), 7682.
(11) Klos, J.; Pakula, T. *Macromolecules* **2004**, *37* (21), 8145.
(12) Meli, L.; Arceo, A.; Green, P. F. *Soft Matter* **2009**, *5* (3), 533–537.
(13) Kim, B. J.; Fredrickson, G. H.; Kramer, E. J. *Macromolecules* **2008**, *41* (2), 436.

(14) Meli, L.; Li, Y.; Lim, K. T.; Johnston, K. P.; Green, P. F. *Macromolecules* **2007**, *40* (18), 6713–6720.
(15) Jandt, K. D.; Heier, J.; Bates, F. S.; Kramer, E. J. *Langmuir* **1996**, *12* (15), 3716–3720.
(16) Wang, H.; Composto, R. J. *J. Chem. Phys.* **2000**, *113* (22), 10386.
(17) Semenov, A. N. *Macromolecules* **1992**, *25* (19), 4967.
(18) Semenov, A. N. *Macromolecules* **1993**, *26* (9), 2273–2281.
(19) Esselink, F. J.; Semenov, A. N.; Ten Brinke, G.; Hadziioannou, G.; Oostergetel, G. T. *Phys. Rev. B: Condens. Matter* **1993**, *48* (18), 13451.
(20) Dai, K. H.; Kramer, E. J. *J. Polym. Sci., Part B: Polym. Phys.* **1994**, *32* (11), 1943.
(21) Fredrickson, G. H.; Liu, A. J.; Bates, F. S. *Macromolecules* **1994**, *27* (9), 2503.